REGULAR ARTICLE

blood advances

Mecom mutation related to radioulnar synostosis with amegakaryocytic thrombocytopenia reduces HSPCs in mice

Koki Nagai,[1] Tetsuya Niihori,[1] Akihiko Muto,[2] Yoshikazu Hayashi,[3] Taiki Abe,[1] Kazuhiko Igarashi,[2] and Yoko Aoki[1]

[1]Department of Medical Genetics and [2]Department of Biochemistry, Tohoku University Graduate School of Medicine, Sendai, Japan; and [3]Division of Functional Structure, Department of Morphological Biology, Fukuoka Dental College, Fukuoka, Japan

Key Points

- Mice with RUSAT-associated *MECOM* mutation were generated to investigate the impact on the phenotype of the organism.
- The mice exhibited thrombocytopenia and reduced hematopoietic stem cells without radioulnar synostosis.

Radioulnar synostosis with amegakaryocytic thrombocytopenia (RUSAT) is an inherited bone marrow failure syndrome characterized by the congenital fusion of the forearm bones. RUSAT is largely caused by missense mutations that are clustered in a specific region of the MDS1 and EVI1 complex locus (*MECOM*). EVI1, a transcript variant encoded by *MECOM*, is a zinc finger transcription factor involved in hematopoietic stem cell maintenance that induce leukemic transformation when overexpressed. Mice with exonic deletions in *Mecom* show reduced hematopoietic stem and progenitor cells (HSPCs). However, the pathogenic roles of RUSAT-associated *MECOM* mutations in vivo have not yet been elucidated. To investigate the impact of the RUSAT-associated MECOM mutation on the phenotype, we generated knockin mice harboring a point mutation (translated into EVI1 p.H752R and MDS1-EVI1 p.H942R), which corresponds to an EVI1 p.H751R and MDS1-EVI1 p.H939R mutation identified in a patient with RUSAT. Homozygous mutant mice died at embryonic day 10.5 to 11.5. Heterozygous mutant mice ($Evi1^{KI/+}$ mice) grew normally without radioulnar synostosis. Male $Evi1^{KI/+}$ mice, aged between 5 and 15 weeks, exhibited lower body weight, and those aged ≥16 weeks showed low platelet counts. Flow cytometric analysis of bone marrow cells revealed a decrease in HSPCs in $Evi1^{KI/+}$ mice between 8 and 12 weeks. Moreover, $Evi1^{KI/+}$ mice showed delayed leukocyte and platelet recovery after 5-fluorouracil–induced myelosuppression. These findings suggest that $Evi1^{KI/+}$ mice recapitulate the bone marrow dysfunction in RUSAT, similar to that caused by loss-of-function *Mecom* alleles.

Introduction

Radioulnar synostosis with amegakaryocytic thrombocytopenia (RUSAT [MIM: PS605432]) is a genetic syndrome characterized by congenital bone marrow failure, radioulnar synostosis (RUS, fusion of the proximal part of the radius with the ulna), congenital heart disease, deafness, and malformation of the digits (such as clinodactyly and brachydactyly).[1-6] Critical bone marrow failure necessitates hematopoietic stem cell transplantation in patients.[1-4,6] Approximately 22 families have been reported to have individuals affected with RUSAT.[1-10] Heterozygous mutations in homeobox A11 (*HOXA11*) and MDS1 and EVI1 complex locus (*MECOM*) have been identified as the underlying cause of RUSAT.[4,10]

MECOM is transcribed into several isoforms with alternative start and splicing sites.[11] The major alternative translation products of *MECOM* are the zinc finger transcription factors EVI1, EVI1 Δ324,

Submitted 29 June 2022; accepted 23 April 2023; prepublished online on *Blood Advances* First Edition 26 April 2023; final version published online 15 September 2023. https://doi.org/10.1182/bloodadvances.2022008462.

Data are available on request from the corresponding author, Tetsuya Niihori (tniihori@med.tohoku.ac.jp).

The full-text version of this article contains a data supplement.

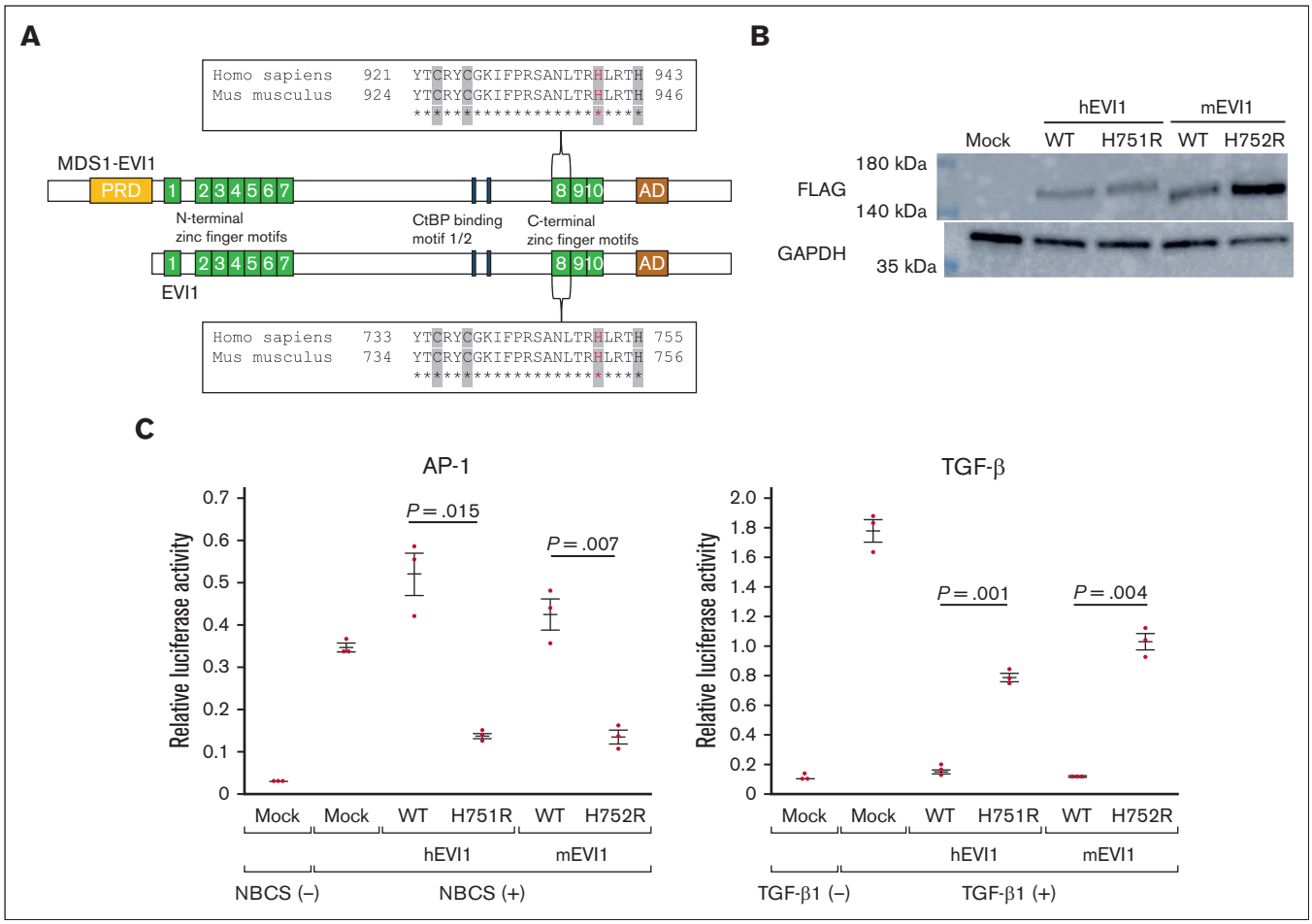

Figure 1. Generation of mutant mice harboring the point mutation translated into EVI1 H752R and MDS1-EVI1 H942R in mice, corresponding to EVI1 H751R and MDS1-EVI1 H939R in humans. (A) The point mutation is located in the eighth zinc finger motifs of EVI1 and MDS1-EVI1. The sequence of the eighth zinc finger motif is given in a box. "C" and "H," shaded in a gray, bind to a zinc ion. EVI1 H751 in humans, MDS1-EVI1 H939 in humans, EVI1 H752 in mice, and MDS1-EVI1 in mice are represented in red letters. (B) Overexpression of C-terminal FLAG-tagged wild-type or mutant hEVI1/mEVI1 in NIH3T3 cells. (C) Luciferase assay for assessing the effects of wild-type or mutant hEVI1/mEVI1 on AP-1 and TGF-β signaling. pCAGGS empty vector (mock) indicates the effectiveness of newborn calf serum or TGF-β1 stimulation. The relationship between the reactions against the stimulation between wild-type and mEVI1 H752R resembles that between wild-type and hEVI1 H751R. Representative data from 3 experiments performed in triplicates are shown. Values are the mean ± standard error of the mean (SEM) of 3 samples of the representative experiment. Underlined numbers denote the *P* value (2-tailed Welch *t* test). Threshold significance level, $P = .05$.

and MDS1-EVI1,[11] of which EVI1 is the best-characterized isoform.[11] EVI1 is a 1051–amino acid protein harboring 7 N-terminal zinc finger motifs at the N-terminus, 3 zinc finger motifs at the C-terminus, the C-terminal binding protein (CtBP) binding motif 1/2, and the acidic domain (Figure 1A).[11,12] MDS1-EVI1 has a PRDF1-RIZ domain added at the N-terminal position of EVI1 (Figure 1A).[11,12] EVI1 interacts with other transcription factors, including GATA1, PU.1, FOS, and SMAD3, to regulate transcription[13] and plays a vital role in ontogenesis and hematopoiesis.[11] *Evi1* is highly expressed in the urinary system, lungs, heart, and developing limbs of mouse embryos.[14] During hematopoiesis, EVI1 binds to the promoter of *GATA2*, which encodes a transcription factor required for the proliferation and survival of early hematopoietic progenitor cells, through the N-terminal zinc finger domain.[15,16] Furthermore, the eighth zinc finger motif of EVI1 represses the activity of RUNX1, another critical transcription factor involved in hematopoiesis.[17] The overexpression of EVI1 or the formation of fusion proteins involving EVI1 because of chromosomal rearrangements at 3q26 leads to hematologic malignancies.[17,18]

Recent studies have identified *MECOM* variants in individuals with congenital bone marrow failure with or without RUS (supplemental Figure 1).[1-9,19-22] In addition, other skeletal anomalies of the forearms and hands, congenital heart diseases, and renal anomalies were also involved with variable penetrance.[1,2,4-7,9,20,22] The term "MECOM-associated syndrome" is proposed to represent this heterogeneous disease.[2] Individuals with congenital bone marrow failure without RUS exhibit nonsense, insertion/deletion, or splicing variants that result in a premature termination codon in *MECOM* (supplemental Figure 1).[1,2,19,20,22-26] RUSAT-associated mutations are located in the eighth and ninth zinc finger motifs, suggesting that RUSAT-associated mutations may have particular intravital effects (supplemental Figure 1).[1-9] Thus far, no RUSAT animal models have been developed. Therefore, the effects of

RUSAT-associated *Mecom* mutations on hematopoiesis and skeletal development have not been analyzed in vivo.

In this study, we generated knockin mice harboring mouse *Mecom* c.2255A>G in XM_006535394.4 (translating into EVI1 [XP_006535457.1] p.H752R and MDS1-EVI1 [NP_001347963.1] p.H942R), corresponding to the pathogenic human *MECOM* c.2252A>G in NM_001105078.4 (translating into EVI1 [NP_001098548.2] p.H751R and MDS1-EVI1 [NP_004982.2] p.H939R; Figure 1A)[4]; we have designated the human EVI1 as hEVI1, the human MDS1-EVI1 as hMDS1-EVI1, the mouse EVI1 as mEVI1, and the mouse MDS1-EVI1 as mMDS1-EVI1. The heterozygous mutant mice ($Evi1^{KI/+}$ mice) exhibited peripheral blood and hematopoietic stem cell (HSC) abnormalities but not RUS, whereas homozygous mutant mice ($Evi1^{KI/KI}$ mice) were embryonic lethal. Our findings indicate that RUSAT-associated *MECOM* missense mutation has a similar effect to loss-of-function alleles in hematopoiesis.

Materials and methods

Plasmid construction, western blot, and luciferase assay

Plasmid generation, western blot, and luciferase assay are described in supplemental Methods. Briefly, pCAGGS plasmids containing complementary DNA encoding the C-terminal FLAG-tagged human EVI1 wild-type, human EVI1 mutant (H751R), mouse Evi1 wild-type, or mouse Evi1 mutant (H752R) were generated. For western blots, NIH3T3 cells (American Type Culture Collection, Manassas, VA) were transfected with one of these plasmids or an empty pCAGGS vector. pAP1-Luc (Agilent Technologies, Santa Clara, CA) or p3TP-lux (Addgene plasmid # 11767) reporter vectors were used in the luciferase assay to assess activator protein 1 (AP-1) or transforming growth factor β (TGF-β) signaling.

Generation of the $Evi1^{KI/+}$ knockin mice

A gene-targeting strategy was used to generate the $Evi1^{KI/+}$ knockin mice. The targeting vector was electroporated into embryonic stem cells derived from C57BL/6 mice. Neomycin selection was performed to isolate homologous recombinant ES cells. Homologous recombination was confirmed using Southern blotting. Blastocysts from BALB/c mice were used for homologous recombinant ES cell injection. ICR mice were used as the foster mothers. The chimeric mice obtained were identified based on their coat colors. The chimeras obtained were crossed with wild-type mice. Selected offspring with the heterozygous targeted allele were then crossed with CAG-Cre mice to excise floxed DNA segments, resulting in the $Evi1^{KI/+}$ *Cre* mice. These mice were crossed with wild-type mice to obtain the $Evi1^{KI/+}$ mice lacking the Cre allele. The primers for Southern blot probes and a schema are provided in supplemental Table 1 and supplemental Figure 2, respectively.

Survival curve, body weight, and digit length of $Evi1^{+/+}$ and $Evi1^{KI/+}$ mice

We evaluated the survival curve and body weight of offspring from 4 pairs of $Evi1^{+/+}$ and $Evi1^{KI/+}$ mice. Nine male $Evi1^{+/+}$, 8 male $Evi1^{KI/+}$, 10 female $Evi1^{+/+}$, and 6 female $Evi1^{KI/+}$ offspring were obtained. The observation period was 1 year. At 5 to 15 weeks, the body weight of the mice was measured once a week. We evaluated 15-week-old $Evi1^{+/+}$ and $Evi1^{KI/+}$ age- and sex-matched littermates ($Evi1^{+/+}$, n = 7; $Evi1^{KI/+}$, n = 7) for digit length. We calculated the average of D3 digit/palm length of both hands of the mice.

Skeletal staining

The staining protocol is provided in supplemental Methods and supplemental Figure 3A. The evaluated mice were as follows: embryonic day 18.5 (E18.5) male $Evi1^{+/+}$ (n = 3), E18.5 female $Evi1^{+/+}$ (n = 5), E18.5 male $Evi1^{KI/+}$ (n = 4), E18.5 female $Evi1^{KI/+}$ (n = 3), postnatal day 0 (P0) male $Evi1^{+/+}$ (n = 3), P0 female $Evi1^{+/+}$ (n = 4), P0 male $Evi1^{KI/+}$ (n = 2), and P0 female $Evi1^{KI/+}$ (n = 4). As described in the study by Chang et al,[27] the ossification level was evaluated using the ossified fraction, which was determined as the ratio of ossified length to the total length of the bone (supplemental Figure 3B).

CBC, megakaryocyte count, and morphology

Complete blood counts (CBCs) of $Evi1^{+/+}$ and $Evi1^{KI/+}$ age- and sex-matched littermates ($Evi1^{+/+}$; n = 10, $Evi1^{KI/+}$; n = 10) were determined using a particle counter (PCE 310; Erma, Tokyo, Japan). Megakaryocyte counts of 13-week-old $Evi1^{+/+}$ and $Evi1^{KI/+}$ mice ($Evi1^{+/+}$, n = 4; $Evi1^{KI/+}$, n = 4) were performed using flow cytometry analysis as described by Winter et al,[28] with modification. The relationship between aging and the presence of megakaryocytes was analyzed using bone marrow cells (BMCs) from $Evi1^{KI/+}$ mice. Megakaryocyte morphology was observed using between 8- and 12-week-old $Evi1^{+/+}$ and $Evi1^{KI/+}$ age- and sex-matched littermates ($Evi1^{+/+}$, n = 4; $Evi1^{KI/+}$, n = 4) and between 10- and 52-week-old $Evi1^{KI/+}$ mice. Detailed protocols are provided in the supplemental Methods.

Flow cytometry of lineage-negative cells

BMCs from 8- to 12-week-old mice were used for this experiment. The combinations of antibodies used for analysis were selected as previously described.[29,30] A detailed protocol is provided in supplemental Methods. A list of the antibodies used is provided in supplemental Table 2.

FU treatment

5-fluorouracil (FU; 200 mg/kg; Towa Pharmaceutical, Osaka, Japan) was administered intraperitoneally to 8-week-old $Evi1^{+/+}$ and $Evi1^{KI/+}$ littermates ($Evi1^{+/+}$, n = 7; $Evi1^{KI/+}$, n = 7). CBC was performed on days 0 (immediately before FU administration), 4, 7, 11, 14, 18, and 21. Peripheral blood was analyzed using a particle counter PCE 310.

Statistics

Graphs were drawn using JMP 16 software (SAS Institute Inc., Cary, NC). Error bars represent the mean ± standard error of the mean. A 2-tailed Welch *t* test was performed using Microsoft Excel (Microsoft Corporation, Redmond, WA) to assess the means of the 2 populations. To assess whether livebirth offspring were born in accordance with the Mendelian ratio, the χ^2 goodness-of-fit test was performed using R version 4.2.2. Statistical significance was set at $P = .05$.

Study approval

Genetic recombination experiments were approved by The Tohoku University Expert Committee on Genetic Recombination Experiments Security. Animal studies were approved by The Institutional

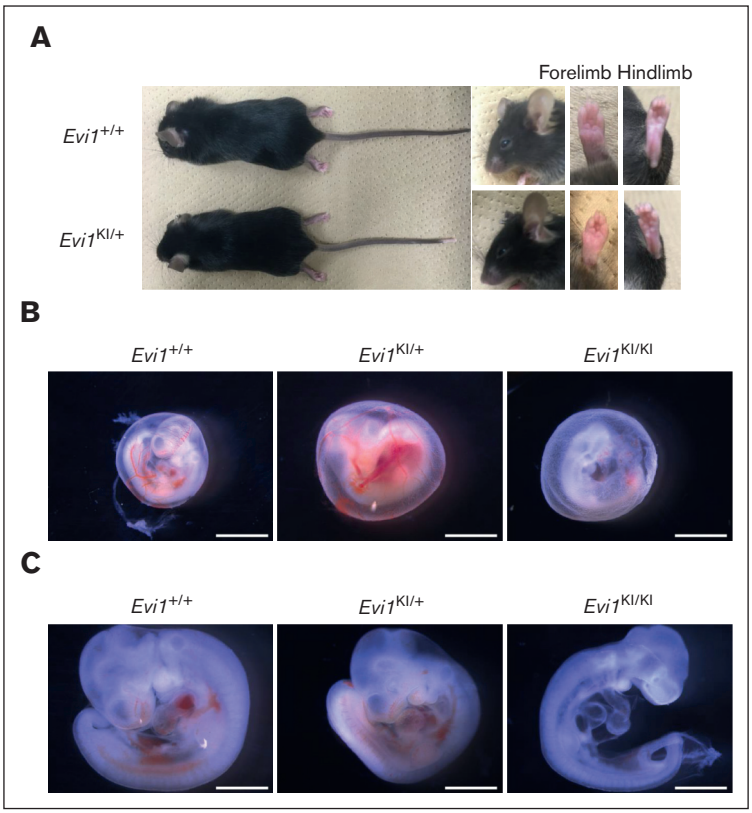

Figure 2. Comparison between *Evi1*$^{KI/+}$ and *Evi1*$^{+/+}$ mice. (A) External morphology of *Evi1*$^{+/+}$ and *Evi1*$^{KI/+}$ mice. Images of 10-week-old male littermates. Gross appearance, face, left forelimb, and left hindlimb of *Evi1*$^{KI/+}$ mice compared with those of *Evi1*$^{+/+}$ mice. There are no external morphological abnormalities. (B) Representative embryos in their yolk sacs at E10.5. The *Evi1*$^{KI/KI}$ embryo has an avascular yolk sac. Bars represent 2.4 mm. (C) Representative *Evi1*$^{+/+}$, *Evi1*$^{KI/+}$, and *Evi1*$^{KI/KI}$ littermates at E10.5. The *Evi1*$^{KI/KI}$ embryo has a flattened head and poor vascularization. Its size is almost the same as the size of *Evi1*$^{+/+}$ and *Evi1*$^{KI/+}$ mice. Bars represent 1.2 mm.

Animal Care and Use Committee of the Tohoku University Environmental & Safety Committee.

Results

Modulation of AP-1 and TGF-β signaling by mEVI1 H752R is similar to that of their human counterparts

Firstly, we evaluated whether the function of mEVI1 H752R, as a transcriptional regulatory factor, is similar to that of hEVI1 H751R, the corresponding human mutant gene. NCBI protein BLAST revealed 93% homology and 95% similarity between hEVI1 and mEVI1.[31,32] The homology and similarity between hMDS1-EVI1 and mMDS1-EVI1 was 93% and 95%, respectively.[31,32] We introduced the wild-type and mutant hEVI1/mEVI1-FLAG into NIH3T3 cells (Figure 1B) and performed luciferase assays to examine the activation of AP-1 and TGF-β signaling, similar to our previous study.[4] We assessed the activation of AP-1 signaling using the pAP1-Luc reporter vector containing specific transcription recognition sequences for AP-1. Under serum stimulation, the relative luciferase activity (RLA) of cells transfected with pAP1-Luc and hEVI1 H751R was lower than that of cells transfected with wild-type hEVI1 (Figure 1C). Similarly, RLA in cells expressing mEVI1 H752R was significantly lower than that in cells expressing wild-type mEVI1 (Figure 1C). Activation of TGF-β signaling was assessed using the p3TP-lux reporter construct containing 3 12-O-tetradecanoylphorbol 13-acetate response elements and a part of the plasminogen activator inhibitor 1 promoter region. The RLA in cells transfected with wild-type hEVI1 was suppressed compared with that in cells transfected with the empty vector (Figure 1C). RLA in cells expressing hEVI1 H751R was remarkably increased compared with that in cells expressing wild-type hEVI1, suggesting a weaker suppressive effect on TGF-β signaling by mutant EVI1 (Figure 1C). We observed the same effect on TGF-β signaling in cells expressing their mouse counterparts (Figure 1C). These results indicate that mEVI1 H752R is, at least in part, functionally similar to hEVI1 H751R.

Generation of *Evi1*$^{KI/+}$ knockin mice

We generated *Evi1*$^{KI/+}$ knockin mice to evaluate the function of mutant *Evi1* in RUSAT using a gene-targeting strategy (supplemental Figures 2 and 4A). Sequence analysis of complementary DNA obtained from the leukocytes, liver, heart, kidney, and the spleen of *Evi1*$^{KI/+}$ mice demonstrated that both the wild-type and H752R *Evi1* messenger RNA were expressed (supplemental Figure 4B). We confirmed the protein expression of MDS1-EVI1 and EVI1 via western blot analysis using embryonic fibroblasts derived from *Evi1*$^{+/+}$, *Evi1*$^{KI/+}$, and *Evi1*$^{KI/KI}$ mice (supplemental Figure 4C). DNA extracted from tails, embryos, embryonic fibroblasts, or yolk sacs was used for genotyping (supplemental Figure 4D). *Evi1*$^{KI/+}$ mice exhibited no gross morphological differences compared with their *Evi1*$^{+/+}$ littermates (Figure 2A). At E10.5, most of the *Evi1*$^{KI/KI}$ mice had avascular yolk sacs, decreased blood vessels in the head and bodies, and flattened heads (Figure 2B-C). They were almost the same size as the *Evi1*$^{+/+}$ and *Evi1*$^{KI/+}$ mice (Figure 2B-C). At E11.5, all the *Evi1*$^{KI/KI}$ mice had died (Table 1). The results indicated that *Evi1*$^{KI/KI}$ mice died at E10.5 through E11.5. In contrast, *Evi1*$^{KI/+}$ mice were born at the expected Mendelian ratio of 1:1 from the *Evi1*$^{+/+}$ and *Evi1*$^{KI/+}$ mice (supplemental Table 3). None of the *Evi1*$^{+/+}$ or *Evi1*$^{KI/+}$ mice died during the 1-year observation period (*Evi1*$^{+/+}$, n = 19 vs *Evi1*$^{KI/+}$,

Table 1. Offspring ratio between *Evi1*$^{KI/+}$ × *Evi1*$^{KI/+}$

	Evi1$^{+/+}$	*Evi1*$^{KI/+}$	*Evi1*$^{KI/KI}$	Total
E9.5	4	7	4	15
E10.5	10	22	3	35
E11.5	7 + 1*	14 + 2	0 + 4	28
E12.5	7	6	0 + 5	18
P0–6	5	12	0	17
Weaning	16	46	0	62

*7 + 1 means that we obtained 7 viable embryos and 1 dead embryo.

n = 14). The daily activities of the *Evi1*$^{KI/+}$ mice were not impaired; they showed no difficulty in feeding or hanging from the wire-netting ceiling of the cages. Between weeks 5 and 7, the *Evi1*$^{KI/+}$ male mice had lower body weights than the *Evi1*$^{+/+}$ male mice of the same age (Figure 3A). Although the difference was not statistically significant, the mean body weight of *Evi1*$^{KI/+}$ male mice was consistently lower than that of *Evi1*$^{+/+}$ male mice from week 8 to 15 (Figure 3A). The *Evi1*$^{KI/+}$ female mice had lower body weights than the *Evi1*$^{+/+}$ female mice that were 5 weeks old (Figure 3A). From 6 to 15 weeks, *Evi1*$^{KI/+}$ female mice had almost the same weight as *Evi1*$^{+/+}$ female mice (Figure 3A). These results indicate that the knockin allele caused no gross morphological abnormalities or persistent lower weight in male mice aged from 5 to 15 weeks.

Some patients with RUSAT and mice with *Mecom* mutation (*Junbo* mice) have malformation of their digits including brachydactyly.[2,4,5,9,22,33] We examined the morphology of the forelimbs and hindlimbs of *Evi1*$^{KI/+}$ mice to examine the effect of this variant on limb development. No extra digits or spurs were observed in *Evi1*$^{KI/+}$ mice (n = 7; Figure 3B). D3 digit/palm length did not show a statistically significant difference between *Evi1*$^{KI/+}$ and *Evi1*$^{+/+}$ mice (Figure 3B).

Evi1$^{KI/+}$ mice exhibit mild ossification delay

The ossification and morphology of the long bones were assessed using double skeletal staining at E18.5 and P0 (Figure 4A; supplemental Figure 3A).[27] All the long bones of the embryos and newborns were morphologically normal. The ossified fraction of the humerus was significantly lower in *Evi1*$^{KI/+}$ mice than in *Evi1*$^{+/+}$ mice at E18.5 (Figure 4B). Although the difference was not statistically significant, the average ossified fraction of other long bones was lower in *Evi1*$^{KI/+}$ mice than that in *Evi1*$^{+/+}$ mice at E18.5 (Figure 4B). In contrast, the ossified fraction in the long bones of *Evi1*$^{KI/+}$ and *Evi1*$^{+/+}$ mice was almost the same as that at P0 (Figure 4B). RUS and skeletal anomalies of the limbs were assessed in 72-week-old *Evi1*$^{KI/+}$ (n = 4) and *Evi1*$^{+/+}$ mice (n = 4). No apparent deformities of the limbs or proximal radioulnar fusion were observed (supplemental Figure 5). These results suggest that a mild ossification delay occurs in the limb bones of *Evi1*$^{KI/+}$ mice at the embryonic stage.

Evi1$^{KI/+}$ mice exhibit low platelet count and reduced HSPC counts

We measured the peripheral blood cell count to evaluate whether *Evi1*$^{KI/+}$ mice developed manifestations similar to those observed in RUSAT. The platelet counts of *Evi1*$^{KI/+}$ mice were significantly lower than those of *Evi1*$^{+/+}$ mice at almost all measurement points from 16 to 50 weeks (Figure 5). Leukocyte counts and hemoglobin levels did not differ significantly between *Evi1*$^{+/+}$ and *Evi1*$^{KI/+}$ mice aged between 4 and 50 weeks (Figure 5). Polyploid megakaryocytes of *Evi1*$^{KI/+}$ mice were reduced compared with those of *Evi1*$^{+/+}$ mice aged 13 weeks (supplemental Figure 6). As megakaryocyte maturation progressed, the difference in megakaryocyte number between *Evi1*$^{+/+}$ and *Evi1*$^{KI/+}$ mice became obvious (supplemental Figure 6). A certain number of megakaryocytes was observed in the bone marrows of *Evi1*$^{KI/+}$ mice aged between 10 and 52 weeks (supplemental Figure 7A). *Evi1*$^{KI/+}$ mice had megakaryocytes with a normal morphology (supplemental Figure 7A-B).

Because RUSAT is characterized by bone marrow failure,[4] we assessed bone marrow hematopoiesis via flow cytometric analysis of bone marrow samples from *Evi1*$^{KI/+}$ mice. BMCs from *Evi1*$^{+/+}$ and *Evi1*$^{KI/+}$ age- and sex-matched littermates aged between 8 and 12 weeks were analyzed. No significant difference was observed in the total number of nucleated cells between the *Evi1*$^{+/+}$ and *Evi1*$^{KI/+}$ mice (supplemental Figure 8). To examine the hematopoietic stem and progenitor cells (HSPCs), the LSK (lineage$^-$, Sca-1$^+$, and c-Kit$^+$) cells were subdivided into HSCs, multipotent progenitors (MPPs), and lymphoid-primed multipotent progenitors (LMPPs). The LSK cell count in *Evi1*$^{KI/+}$ mice was found to be significantly lower than that in wild-type mice (1.72×10^5 cells in *Evi1*$^{+/+}$ mice vs 1.06×10^5 cells in *Evi1*$^{KI/+}$ mice; $P = .034$ using 2-tailed Welch *t* test; Figure 6A-B). The cell counts of HSC, MPP, and LMPPs were lower in *Evi1*$^{KI/+}$ mice than in *Evi1*$^{+/+}$ mice (Figure 6A-B). To examine myeloid progenitor cells, LK (lineage$^-$, Sca-1$^-$, and c-Kit$^+$) cells were subdivided into common myeloid progenitors (CMPs), megakaryocyte-erythrocyte progenitors (MEPs), and granulocyte-monocyte progenitors (GMPs). The numbers of LK, CMP, MEP, and GMP cells in *Evi1*$^{KI/+}$ mice were similar to those in wild-type mice (Figure 6C-D). These results suggest that the number of HSPCs was decreased and that the number of myeloid progenitor cells was not altered in *Evi1*$^{KI/+}$ mice compared with those in *Evi1*$^{+/+}$ mice (supplemental Figure 9).[34]

Evi1$^{KI/+}$ mice show impaired leukocyte and platelet count recovery from myelosuppression

FU kills BMCs and spares long-term HSCs.[35] After the BMC count is reduced, FU works in the bone marrow niche to regenerate HSCs.[36] To evaluate hematopoietic recovery from myelosuppression, FU was administered to the 8-week-old *Evi1*$^{+/+}$ and *Evi1*$^{KI/+}$ age- and sex-matched littermates. We tracked the CBC of the mice. The decreasing trend in peripheral blood cells after FU administration was similar between *Evi1*$^{+/+}$ and *Evi1*$^{KI/+}$ mice (Figure 7). *Evi1*$^{KI/+}$ mice showed delayed platelet and leukocyte count recovery compared with *Evi1*$^{+/+}$ mice (Figure 7). Although the difference was not significant, hemoglobin recovery in the *Evi1*$^{KI/+}$ mice was delayed compared with that in the *Evi1*$^{+/+}$ mice (Figure 7).

Discussion

In this study, we generated mice with a RUSAT-associated *Mecom* mutation. *Evi1*$^{KI/KI}$ mice died at E10.5 to 11.5, and adult *Evi1*$^{KI/+}$ mice did not exhibit clear RUS. The ossification of long bones in the *Evi1*$^{KI/+}$ mice was delayed at E18.5 but was almost the same at P0, compared with that in *Evi1*$^{+/+}$ mice. The platelet and HSPC counts of *Evi1*$^{KI/+}$ mice were lower than those of *Evi1*$^{+/+}$ mice, whereas the myeloid progenitor cell counts did not differ between *Evi1*$^{KI/+}$

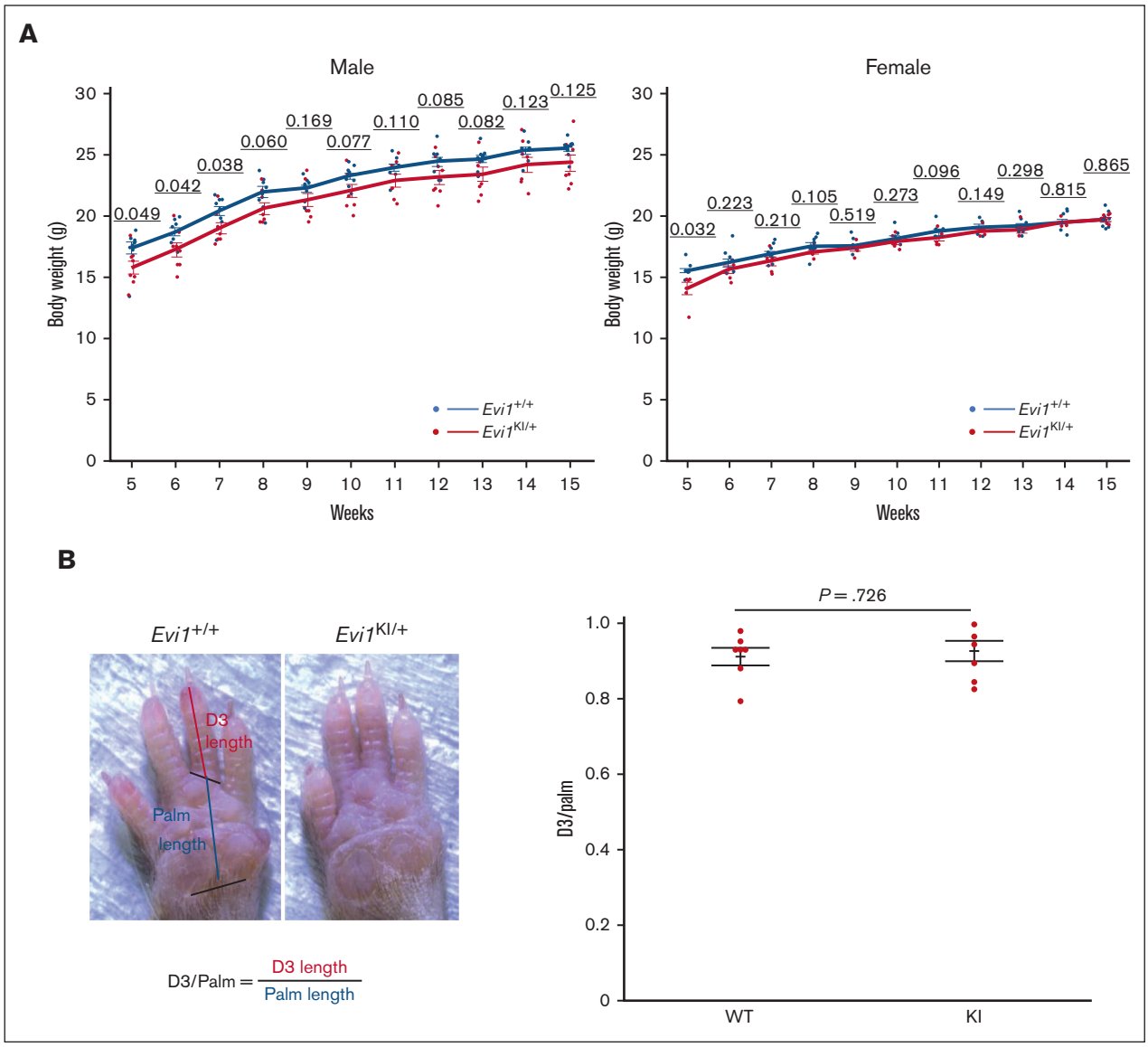

Figure 3. Comparison between *Evi1*$^{KI/+}$ and *Evi1*$^{+/+}$ mice. (A) Body weight of male and female *Evi1*$^{+/+}$ and *Evi1*$^{KI/+}$ mice. Values are the mean ± SEM of each group (male *Evi1*$^{+/+}$, n = 9; male *Evi1*$^{KI/+}$, n = 8; female *Evi1*$^{+/+}$, n = 10; and female *Evi1*$^{KI/+}$, n = 6). In male mice aged between 5 and 7 weeks, *Evi1*$^{KI/+}$ mice had significantly lower body weights than *Evi1*$^{+/+}$ mice. In female mice aged 5 weeks, *Evi1*$^{KI/+}$ mice had significantly lower body weights than *Evi1*$^{+/+}$ mice. (B) The photograph shows the right palm of *Evi1*$^{+/+}$ and *Evi1*$^{KI/+}$ mice. D3/palm was calculated by dividing D3 length by palm length. D3/palm of *Evi1*$^{+/+}$ and *Evi1*$^{KI/+}$ age- and sex-matched littermates (*Evi1*$^{+/+}$, n = 7; *Evi1*$^{KI/+}$, n = 7). There is no significant difference between *Evi1*$^{+/+}$ and *Evi1*$^{KI/+}$ age- and sex-matched littermates. Threshold significance level, $P = .05$ (2-tailed Welch *t* test). Underlined numbers denote the *P* value. Values are the mean ± SEM of each group. WT, *Evi1*$^{+/+}$ mice; KI, *Evi1*$^{KI/+}$ mice.

and *Evi1*$^{+/+}$ mice. Furthermore, *Evi1*$^{KI/+}$ mice presented delayed recovery of leukocyte and platelet counts after FU treatment. Although the phenotypic similarity to RUSAT was limited, the hematopoietic defects in these mice support the pathogenicity of the introduced missense variant at the eighth zinc finger motif.

The heterozygous *Mecom* mutation in *Evi1*$^{KI/+}$ mice corresponds to RUSAT-associated mutation in humans. Five *Mecom* mutant mice were generated (Table 2).[37-41] Four of them had deletions of exon 1 of *Mds1-Evi1* or exons 3, 4, or 7 of *Evi1*; abbreviations of these mice are defined in Table 2.[37-39,41] Affected translation products of *Mecom* depend on the deletions (Table 2).[37-39,41]

Junbo mice have a missense mutation in mEVI1 (p.N783I), which is located in the ninth zinc finger motif (Table 2),[40] and are a model organism of otitis media. mEVI1 N783I corresponds to hEVI1 N782I, which has not been reported in patients with RUSAT. To the best of our knowledge, this is the first report of genetically authentic mice that expresses a mutation identified in patients with RUSAT.

The LSK cell and HSC counts in *Evi1*$^{KI/+}$ mice were lower than those in wild-type mice between 8 and 12 weeks of age. *Evi1*$^{\Delta 3/+}$ or *Evi1*$^{\Delta 4/+}$ mice showed decreased LSK cell count in the fetal liver at E14.5.[37,38] *Evi1*$^{\Delta 4/+}$ mice showed almost extinct long-term

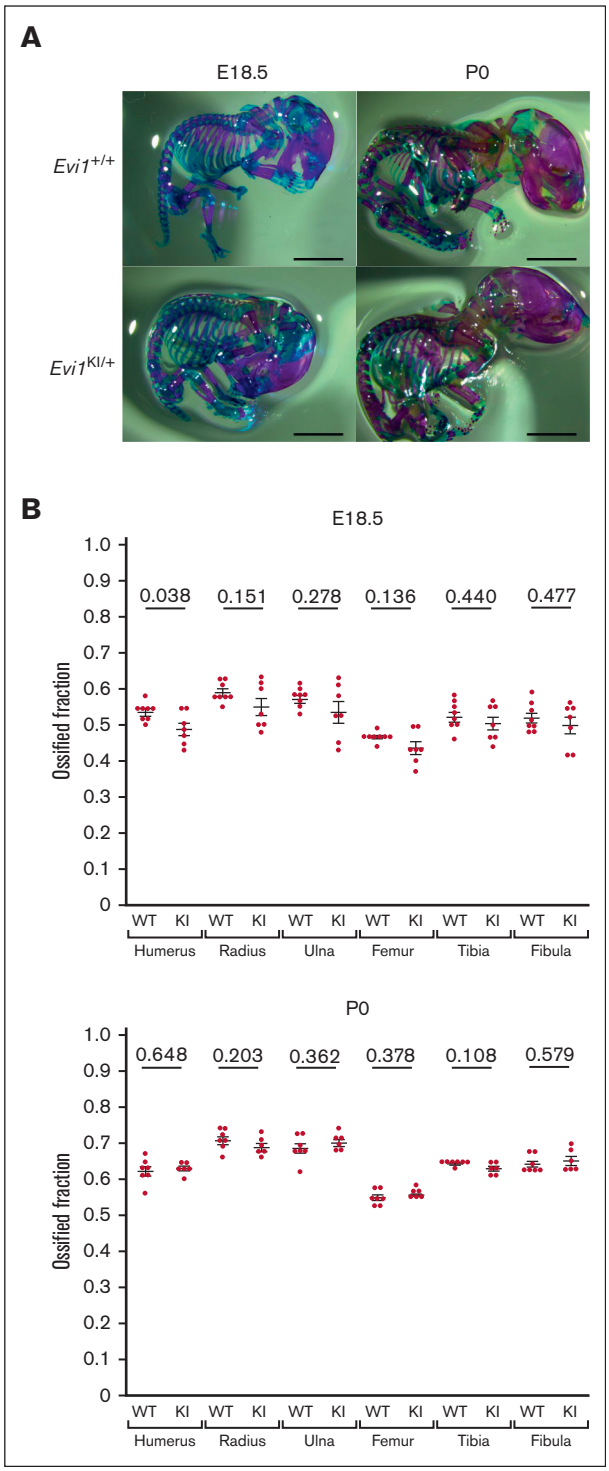

Figure 4. *Evi1*$^{KI/+}$ mice show mild ossification delay. (A) Alcian blue and Alizarin red staining of *Evi1*$^{+/+}$ mice and *Evi1*$^{KI/+}$ mice at E18.5 and P0. Bars represent 5 mm. The ossified fraction was used to evaluate ossification, based on the study by Chang et al.[24] (B) Ossification of *Evi1*$^{+/+}$ and *Evi1*$^{KI/+}$ mice. At E18.5, although only the comparison of the humeral ossification was statistically significant, *Evi1*$^{KI/+}$ mice (n = 7) exhibited delayed ossification compared with *Evi1*$^{+/+}$ mice (n = 8). At P0, there was no significant difference between the ossification of *Evi1*$^{+/+}$ mice (n = 7) and *Evi1*$^{KI/+}$ mice (n = 6). Threshold significance level, $P = .05$ (2-tailed Welch *t* test). Underlined numbers denote the *P* value. Values are the mean ± SEM of each group. WT, *Evi1*$^{+/+}$ mice; KI, *Evi1*$^{KI/+}$ mice.

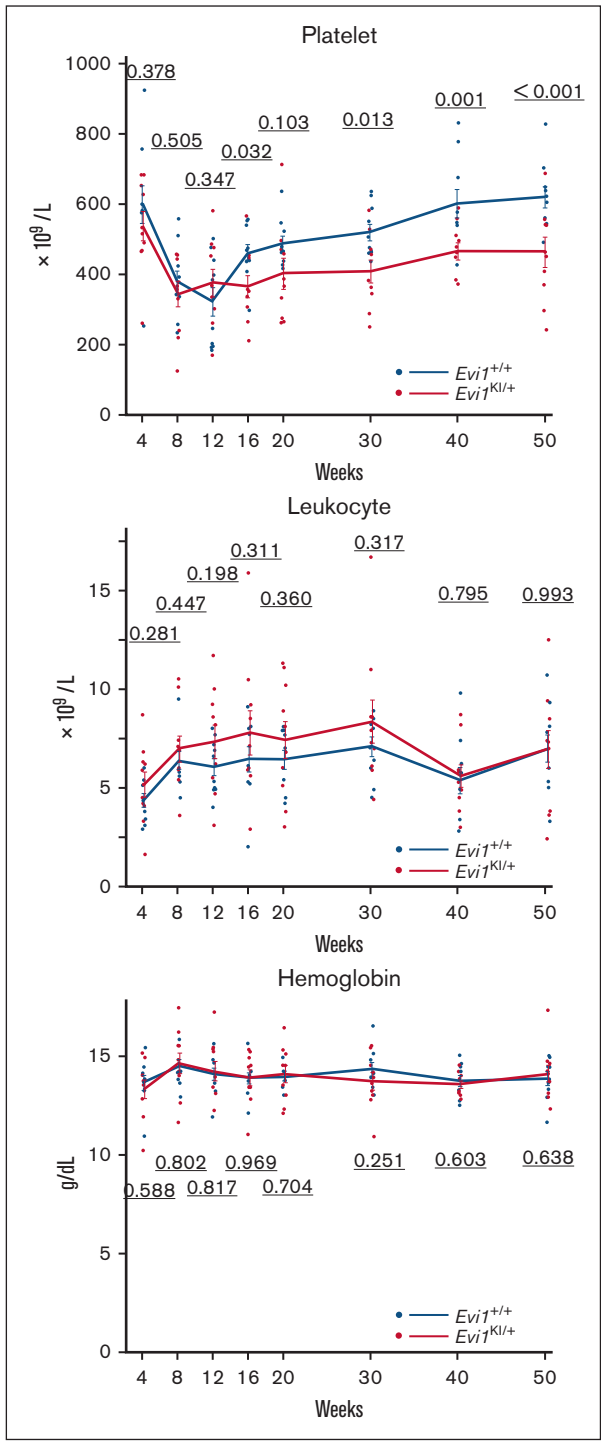

Figure 5. *Evi1*$^{KI/+}$ mice show decreased platelet count with age. (A) Peripheral blood cells of *Evi1*$^{+/+}$ and *Evi1*$^{KI/+}$ age- and sex-matched littermates (*Evi1*$^{+/+}$, n = 10; *Evi1*$^{KI/+}$, n = 10). The platelet count of *Evi1*$^{KI/+}$ mice was significantly lower than that of *Evi1*$^{+/+}$ mice at 16, 30, 40, and 50 weeks of age. Threshold significance level, $P = .05$ (2-tailed Welch *t* test). Underlined numbers denote the *P* value. Values are the mean ± SEM of each group.

HSCs in their bone marrow.[42] EVI1 is involved in HSC maintenance and cellular adhesion to the bone marrow niche via upregulation of *ADGRG1* expression.[43,44] MDS1-EVI1 plays an

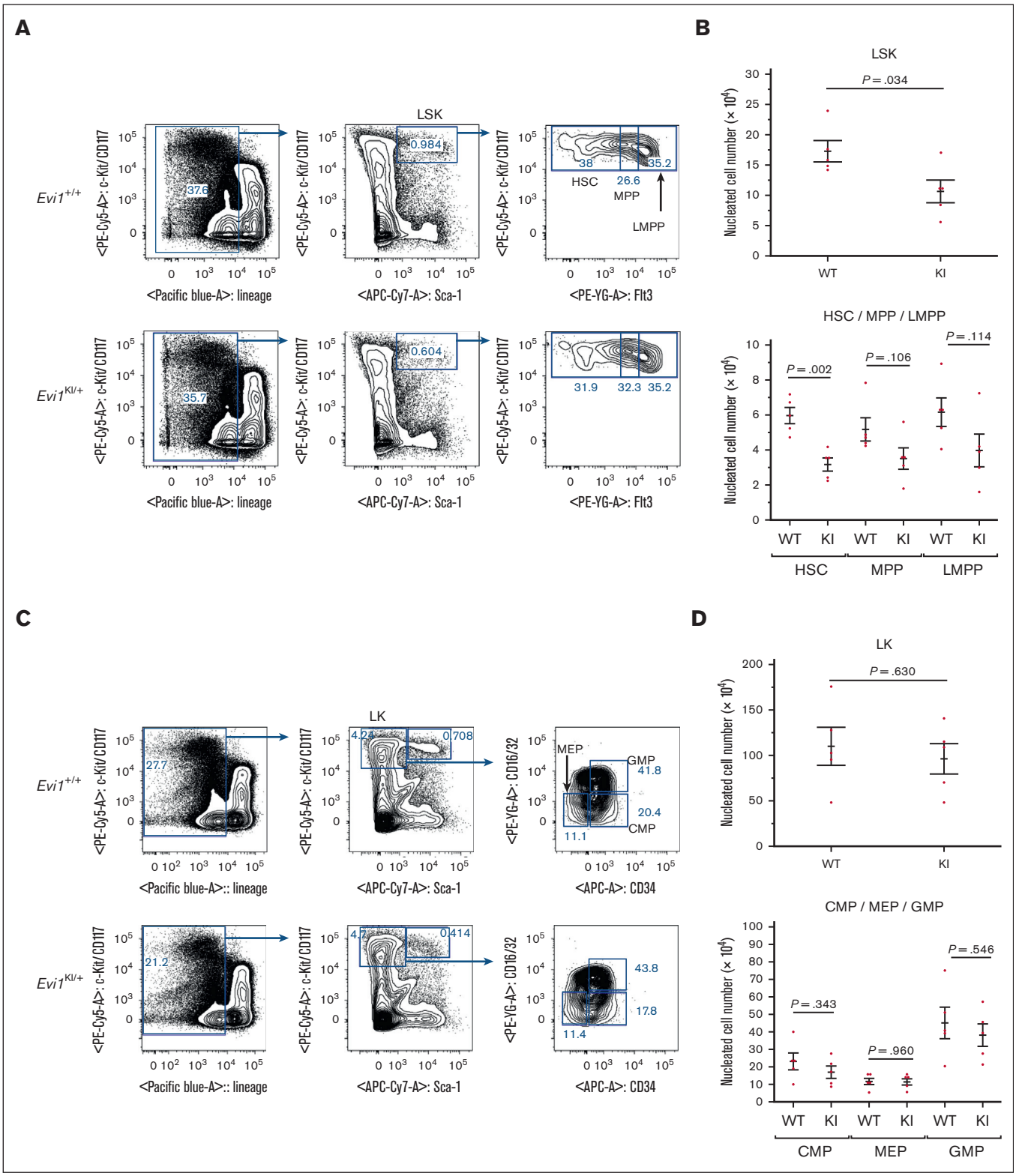

Figure 6. *Evi1*$^{KI/+}$ mice show impaired HSPCs. (A) Flow cytometric analysis of HSPCs. BMCs were obtained from the bilateral femur and tibia of *Evi1*$^{+/+}$ and *Evi1*$^{KI/+}$ age- and sex-matched littermates. The LSK compartment of *Evi1*$^{KI/+}$ mice was visually reduced compared with that of *Evi1*$^{+/+}$ mice. Representative data from 5 experiments are shown. (B) The number of LSK cells and their components. The LSK cell count of *Evi1*$^{KI/+}$ mice (n = 5) was significantly lower than that of *Evi1*$^{+/+}$ mice (n = 5). (C) Flow cytometric analysis of myeloid progenitor cells. The LK compartment of *Evi1*$^{KI/+}$ mice resembled that of *Evi1*$^{+/+}$ mice. Representative data from 5 experiments are shown. (D) The number of LK cells and its components. There was no significant difference between the number of LK cells and their components of *Evi1*$^{KI/+}$ mice (n = 5) and those of *Evi1*$^{+/+}$ mice (n = 5). Threshold significance level, $P = .05$ (2-tailed Welch *t* test). Underlined numbers denote the *P* value. Values are the mean ± SEM of each group. WT, *Evi1*$^{+/+}$ mice; KI, *Evi1*$^{KI/+}$ mice.

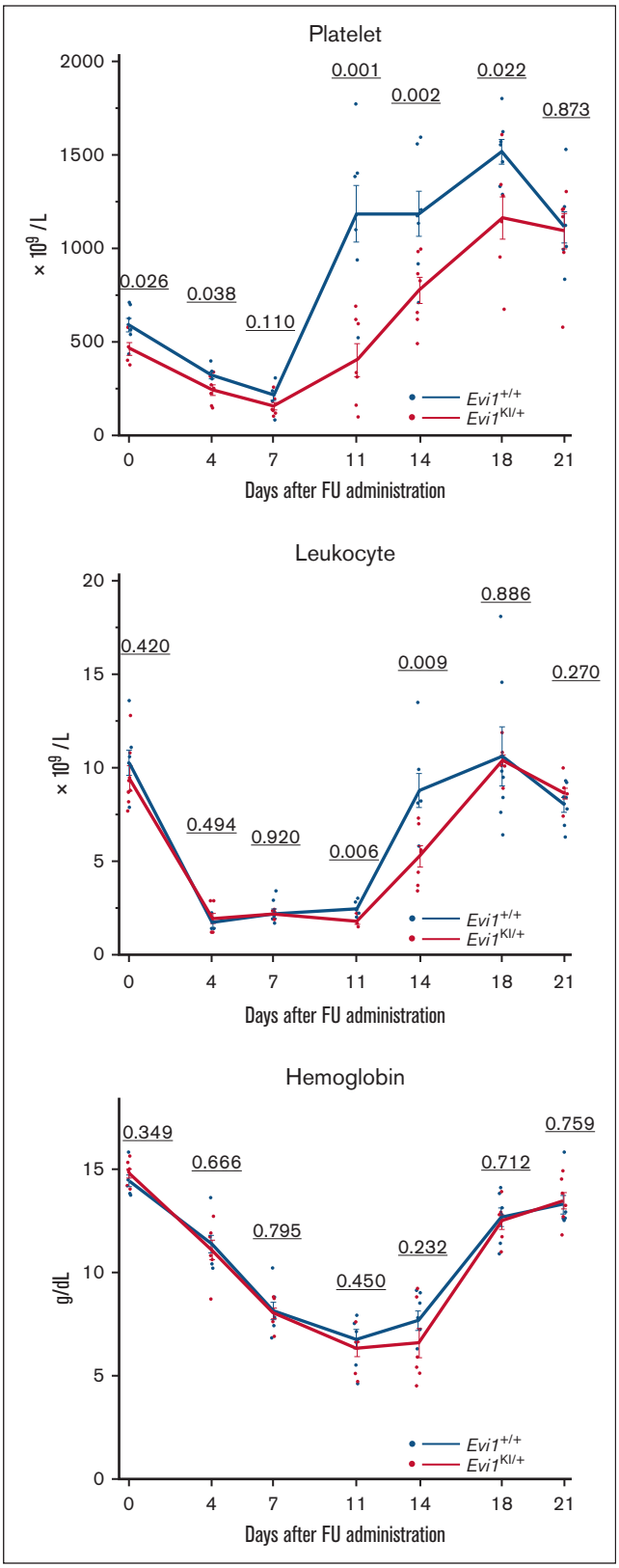

Figure 7. *Evi1*$^{KI/+}$ mice show low platelet count and delayed leukocyte and platelet recovery from FU treatment. The peripheral blood cells of *Evi1*$^{+/+}$ and *Evi1*$^{KI/+}$ age- and sex-matched littermates after FU administration (*Evi1*$^{+/+}$, n = 7 vs *Evi1*$^{KI/+}$, n = 7).

important role in long-term HSCs.[41] *Mds1*$^{\Delta/\Delta}$ mice reduce LSK cells and HSCs as seen in *Evi1*$^{KI/+}$ mice.[41] Therefore, EVI1 and MDS1-EVI1 mutations are assumed to participate in impaired HSC maintenance. Unlike the LSK cell count, the LK cell count of *Evi1*$^{KI/+}$ mice was normal. Recent studies have shown that progenitors independent of traditional HSCs drive hematopoiesis in embryos[45] and adults.[46] *Evi1*$^{+/-}$ mouse embryos exhibited highly decreased HSCs and normal progenitors (CMPs, GMPs, and MEPs),[45] resembling our observations. These results indicate that the EVI1 mutation causes a bias in hematopoietic differentiation.

Evi1$^{KI/+}$ mice showed lower platelet counts at 16 weeks and later in age, although their progenitor MEPs were comparable with those of *Evi1*$^{+/+}$ mice between 8 and 12 weeks of age. Although the reason for the differences in counts within the lower-level hierarchy is still unknown, the decreased contribution of HSC-independent hematopoiesis with age[46] could explain, at least in part, the age dependency of the lower platelet counts after 12 weeks of age. When focusing on the differentiation stage between MEPs and platelets, *Evi1*$^{KI/+}$ mice showed reduced counts of mature polyploid megakaryocytes at 13 weeks of age. Although TGF-β is obviously not the only factor responsible for the complex process in megakaryopoiesis and platelet production,[47] it is possible that insufficient suppression of TGF-β signaling by mutant EVI1 reduced megakaryocyte polyploidization, based on the knowledge that TGF-β1 suppresses their polyploidization.[48] The vast majority of platelet-producing megakaryocytes are ≥16N,[49,50] and thus inhibited polyploidization results in lower thrombocyte counts. TGF-β is a well-known regulator of HSC lineage determination, self-renewal, and differentiation in development.[51] When TGF-β signaling was blocked at the hematopoietic regeneration phase after FU treatment, recovery from cytopenia was shortened.[52] One of the reasons for delayed recovery from FU-induced cytopenia in *Evi1*$^{KI/+}$ mice also may be associated with insufficient inhibition of TGF-β signaling.

The *Evi1*$^{KI/KI}$ mice were embryonic lethal from E10.5 to 11.5, an earlier stage than that of *Evi1*$^{\Delta4/\Delta4}$ mice (whose protein isoforms of MECOM are null) and almost the same as that of *Evi1*$^{\Delta7/\Delta7}$ mice (which have null mEVI1, normal mEVI1 Δ324, and null mMDS1-EVI1) (Table 2).[38,39] *Mds1*$^{\Delta/\Delta}$ mice, which have normal mEVI1, normal mEVI1 Δ324, and null mMDS1-EVI1, were not embryonic lethal (Table 2).[41] The number of *Evi1*$^{\Delta3/\Delta3}$ mice, which have truncated mEVI1, truncated mEVI1 Δ324, and null mMDS1-EVI1, were within a typical Mendelian ratio at birth but died within 3 days (Table 2).[37] Many homozygous *Junbo* mice died at E18.5, although their background was not C57BL/6 but C3H/HeN.[40] Overall, mEVI1 H752R induced a severe defect during ontogenesis, similar to loss-of-function alleles.

Evi1$^{KI/+}$ mice exhibited ossification delay at E18.5 with no difference in their ossification levels at P0. Fifteen-week-old *Evi1*$^{KI/+}$ mice did not exhibit short digit length in addition to extra digits. Our luciferase assay indicated that mEVI1 H752R had an impaired ability to inhibit TGF-β signaling or response to AP-1 signaling.

Figure 7 (continued) The platelet and leukocyte count recovery of *Evi1*$^{KI/+}$ mice was slow and delayed. Platelet count rebound of *Evi1*$^{KI/+}$ mice was milder than that of *Evi1*$^{+/+}$ mice. Values are the mean ± SEM of each group. Threshold significance level, $P = .05$ (2-tailed Welch *t* test).

Table 2. Previously reported mice with *Mecom* mutation

	Mds1-Evi1 knockout	Exon 3 deletion	Exon 4 deletion	Exon 7 deletion	*Junbo* mice	This study
Reference	41	37	38, 42	39, 44	40	–
Genetic background	C57BL/6	C57BL/6	C57BL/6	C57BL/6J	C3H/HeN	C57BL/6J
mEVI1 (XM_006535394.4)	Normal	42-aa truncation at the N-terminus	Null	Null	c.2348A>T (p.N783I)	c.2255A>G (p.H752R)
mEVI1 Δ324 (NM_007963.2)	Normal	42-aa truncation at the N-terminus	Null	Normal	c.1346A>T (p.N449I)	c.1253A>G (p.H418R)
mMDS1-EVI1 (NM_001361034.3)	Null	Null	Null	Null	c.2918A>T (p.N973I)	c.2825A>G (p.H942R)
Heterozygous mice	*Mds1*$^{\Delta/+}$ mice	*Evi1*$^{\Delta3/+}$ mice	*Evi1*$^{\Delta4/+}$ mice	*Evi1*$^{\Delta7/+}$ mice		*Evi1*$^{KI/+}$ mice
Homozygous mice	*Mds1*$^{\Delta/\Delta}$ mice	*Evi1*$^{\Delta3/\Delta3}$ mice	*Evi1*$^{\Delta4/\Delta4}$ mice	*Evi1*$^{\Delta7/\Delta7}$ mice		*Evi1*$^{KI/KI}$ mice
Lethality of homozygous mice	No (some mice die from malocclusion)	P0-3	E13.5-16.5	About E10.5	E10.5 (17%) E18.5-birth (83%)	E10.5-11.5
Hematologic abnormalities of mutant mice	(Homozygous) Reduced platelets and increased leukocytes in adult mice Reduced LSK cells and HSCs and increased GMPs in bone marrow	(Heterozygous) Reduced LSK and CD34$^+$ LK cells in fetal livers	(Heterozygous) Reduced LSK and CD34$^+$ LK cells in fetal livers Almost extinct long-term HSCs in bone marrow		(Heterozygous) Increased ratio of immature neutrophils to the total neutrophils	(Heterozygous) Reduced LSK cells in bone marrow from 8 to 12 weeks old Reduced platelets of adult mice

aa, amino acid.

TGF-β signaling induces the proliferation and differentiation of osteoprogenitor cells into osteoblasts.[53] It also inhibits the maturation and calcification of osteoblasts and their transition into osteocytes.[53] FOS, a component of the AP-1 heterodimer, is involved in differentiating chondrocytes.[54] Although many molecules are associated with bone ossification, modulation of TGF-β and AP-1 signaling by mutant EVI1 may be involved in a mild ossification delay. The limb phenotypic differences between the *Evi1*$^{KI/+}$ mice and *Junbo* mice might be because of strain differences or different functional properties of the variants.

Our results demonstrate the functional significance of a missense *Mecom* mutation corresponding to a human mutation identified in an individual with RUSAT in vivo. Mice with a RUSAT-associated *Mecom* mutation may enable us to study and identify new roles for *Mecom* in hematopoiesis.

Acknowledgments

The authors thank Koichi Onodera and Hisayuki Yokoyama for their helpful comments on hematopoietic differentiation in mice; Jun-ichi Miyazaki for pCAGGS; and Joan Massague and Jeff Wrana for p3TP-lux (Addgene plasmid #11767). The authors also thank Yoko Tateda, Kumi Kato, and Riyo Takahashi for their technical assistance. They thank the Biomedical Research Unit of Tohoku University Hospital and the Biomedical Research Core of Tohoku University Graduate School of Medicine for their technical support.

This study was supported by Grants-in-Aid for Research on Rare and Intractable Diseases (H26-itaku[nan]-ippan-082) (T.N.) from the Ministry of Health, Labour and Welfare of Japan; the Practical Research Project for Rare/Intractable Diseases (15ek0109067h0002, 16ek0109067h0003) (T.N. and Y.A.) from the Japan Agency for Medical Research and Development; the Medical Research grant and the Medical Research Continuous grant (T.N.) from the Takeda Science Foundation; and JSPS KAKENHI grants JP17K10045 and JP20H03637 (T.N.).

Authorship

Contribution: Y.A. and T.N. designed the study; K.N. and A.M. performed the experiments; K.N., T.A., T.N., and Y.A. analyzed and interpreted the experiments; A.M., Y.H., and K.I. analyzed and interpreted the flow cytometry data of LK and LSK analysis; K.N., T.N., and Y.A. wrote the manuscript; and all authors have read and approved the final manuscript.

Conflict-of-interest disclosure: The authors declare no competing financial interests.

ORCID profiles: T.N., 0000-0002-2118-9776; Y.H., 0000-0001-8834-7946; T.A., 0000-0001-6580-3734; K.I., 0000-0002-2470-2475.

Correspondence: Tetsuya Niihori, Department of Medical Genetics, Tohoku University Graduate School of Medicine, 1-1 Seiryo-machi, Sendai 980-8574, Japan; email: tniihori@med.tohoku.ac.jp; and Yoko Aoki, Department of Medical Genetics, Tohoku University Graduate School of Medicine, 1-1 Seiryo-machi, Sendai 980-8574, Japan; email: aokiy@med.tohoku.ac.jp.

References

1. Bluteau O, Sebert M, Leblanc T, et al. A landscape of germ line mutations in a cohort of inherited bone marrow failure patients. *Blood*. 2018;131(7):717-732.

2. Germeshausen M, Ancliff P, Estrada J, et al. MECOM-associated syndrome: a heterogeneous inherited bone marrow failure syndrome with amegakaryocytic thrombocytopenia. *Blood Adv*. 2018;2(6):586-596.

3. Lord SV, Jimenez JE, Kroeger ZA, et al. A MECOM variant in an African American child with radioulnar synostosis and thrombocytopenia. *Clin Dysmorphol*. 2018;27(1):9-11.
4. Niihori T, Ouchi-Uchiyama M, Sasahara Y, et al. Mutations in MECOM, encoding oncoprotein EVI1, cause radioulnar synostosis with amegakaryocytic thrombocytopenia. *Am J Hum Genet*. 2015;97(6):848-854.
5. Ripperger T, Hofmann W, Koch JC, et al. MDS1 and EVI1 complex locus (MECOM): a novel candidate gene for hereditary hematological malignancies. *Haematologica*. 2018;103(2):e55-e58.
6. Walne A, Tummala H, Ellison A, et al. Expanding the phenotypic and genetic spectrum of radioulnar synostosis associated hematological disease. *Haematologica*. 2018;103(7):e284-e287.
7. Al-Abboh H, Zahra A, Adekile A. A novel MECOM variant associated with congenital amegakaryocytic thrombocytopenia and radioulnar synostosis. *Pediatr Blood Cancer*. 2022;69(12):e29761.
8. Loganathan A, Munirathnam D, Ravikumar T. A novel mutation in the MECOM gene causing radioulnar synostosis with amegakaryocytic thrombocytopenia (RUSAT-2) in an infant. *Pediatr Blood Cancer*. 2019;66(4):e27574.
9. Niihori T, Tanoshima R, Sasahara Y, et al. Phenotypic heterogeneity in individuals with MECOM variants in 2 families. *Blood Adv*. 2022;6(18):5257-5261.
10. Thompson AA, Nguyen LT. Amegakaryocytic thrombocytopenia and radio-ulnar synostosis are associated with HOXA11 mutation. *Nat Genet*. 2000;26(4):397-398.
11. Wieser R. The oncogene and developmental regulator EVI1: expression, biochemical properties, and biological functions. *Gene*. 2007;396(2):346-357.
12. Fears S, Mathieu C, Zeleznik-Le N, Huang S, Rowley JD, Nucifora G. Intergenic splicing of MDS1 and EVI1 occurs in normal tissues as well as in myeloid leukemia and produces a new member of the PR domain family. *Proc Natl Acad Sci U S A*. 1996;93(4):1642-1647.
13. Bard-Chapeau EA, Gunaratne J, Kumar P, et al. EVI1 oncoprotein interacts with a large and complex network of proteins and integrates signals through protein phosphorylation. *Proc Natl Acad Sci U S A*. 2013;110(31):E2885-2894.
14. Perkins AS, Mercer JA, Jenkins NA, Copeland NG. Patterns of Evi-1 expression in embryonic and adult tissues suggest that Evi-1 plays an important regulatory role in mouse development. *Development*. 1991;111(2):479-487.
15. Tsai FY, Orkin SH. Transcription factor GATA-2 is required for proliferation/survival of early hematopoietic cells and mast cell formation, but not for erythroid and myeloid terminal differentiation. *Blood*. 1997;89(10):3636-3643.
16. Yatsula B, Lin S, Read AJ, et al. Identification of binding sites of EVI1 in mammalian cells. *J Biol Chem*. 2005;280(35):30712-30722.
17. Senyuk V, Sinha KK, Li D, Rinaldi CR, Yanamandra S, Nucifora G. Repression of RUNX1 activity by EVI1: a new role of EVI1 in leukemogenesis. *Cancer Res*. 2007;67(12):5658-5666.
18. Birdwell C, Fiskus W, Kadia TM, DiNardo CD, Mill CP, Bhalla KN. EVI1 dysregulation: impact on biology and therapy of myeloid malignancies. *Blood Cancer J*. 2021;11(3):64.
19. Datta SS, Basu S, Ghara N, Kole P, Khemka P. Utility of platelet cross-matching in a case of neonatal alloimmune thrombocytopenia associated with a de novo MECOM variant. *Blood Res*. 2021;56(1):53-56.
20. Deliloğlu B, Tufekci O, Tuzun F, et al. A novel Mecom gene mutation associated with amegakaryocytic thrombocytopenia in a premature infant. *Turk J Pediatr*. 2022;64(4):736-740.
21. Osumi T, Tsujimoto SI, Nakabayashi K, et al. Somatic MECOM mosaicism in a patient with congenital bone marrow failure without a radial abnormality. *Pediatr Blood Cancer*. 2018;65(6):e26959.
22. Weizmann D, Pincez T, Roussy M, Vaillancourt N, Champagne J, Laverdiere C. New MECOM variant in a child with severe neonatal cytopenias spontaneously resolving. *Pediatr Blood Cancer*. 2020;67(5):e28215.
23. Bouman A, Knegt L, Groschel S, et al. Congenital thrombocytopenia in a neonate with an interstitial microdeletion of 3q26.2q26.31. *Am J Med Genet A*. 2016;170A(2):504-509.
24. Kjeldsen E, Veigaard C, Aggerholm A, Hasle H. Congenital hypoplastic bone marrow failure associated with a de novo partial deletion of the MECOM gene at 3q26.2. *Gene*. 2018;656:86-94.
25. Nielsen M, Vermont CL, Aten E, et al. Deletion of the 3q26 region including the EVI1 and MDS1 genes in a neonate with congenital thrombocytopenia and subsequent aplastic anaemia. *J Med Genet*. 2012;49(9):598-600.
26. van der Veken LT, Maiburg MC, Groenendaal F, et al. Lethal neonatal bone marrow failure syndrome with multiple congenital abnormalities, including limb defects, due to a constitutional deletion of 3' MECOM. *Haematologica*. 2018;103(4):e173-e176.
27. Chang R, Petersen JR, Niswander LA, Liu A. A hypomorphic allele reveals an important role of inturned in mouse skeletal development. *Dev Dyn*. 2015;244(6):736-747.
28. Winter O, Moser K, Mohr E, et al. Megakaryocytes constitute a functional component of a plasma cell niche in the bone marrow. *Blood*. 2010;116(11):1867-1875.
29. Itoh-Nakadai A, Matsumoto M, Kato H, et al. A Bach2-Cebp gene regulatory network for the commitment of multipotent hematopoietic progenitors. *Cell Rep*. 2017;18(10):2401-2414.
30. Kato H, Itoh-Nakadai A, Matsumoto M, et al. Infection perturbs Bach2- and Bach1-dependent erythroid lineage 'choice' to cause anemia. *Nat Immunol*. 2018;19(10):1059-1070.

31. Altschul SF, Madden TL, Schaffer AA, et al. Gapped BLAST and PSI-BLAST: a new generation of protein database search programs. *Nucleic Acids Res*. 1997;25(17):3389-3402.
32. Altschul SF, Wootton JC, Gertz EM, et al. Protein database searches using compositionally adjusted substitution matrices. *FEBS J*. 2005;272(20):5101-5109.
33. Li J, Glover JD, Zhang H, et al. Limb development genes underlie variation in human fingerprint patterns. *Cell*. 2022;185(1):95-112.e18.
34. Doulatov S, Notta F, Laurenti E, Dick JE. Hematopoiesis: a human perspective. *Cell Stem Cell*. 2012;10(2):120-136.
35. Lerner C, Harrison DE. 5-Fluorouracil spares hemopoietic stem cells responsible for long-term repopulation. *Exp Hematol*. 1990;18(2):114-118.
36. Jeong SY, Kim JA, Oh IH. The adaptive remodeling of stem cell niche in stimulated bone marrow counteracts the leukemic niche. *Stem Cells*. 2018;36(10):1617-1629.
37. Bard-Chapeau EA, Szumska D, Jacob B, et al. Mice carrying a hypomorphic Evi1 allele are embryonic viable but exhibit severe congenital heart defects. *PLoS One*. 2014;9(2):e89397.
38. Goyama S, Yamamoto G, Shimabe M, et al. Evi-1 is a critical regulator for hematopoietic stem cells and transformed leukemic cells. *Cell Stem Cell*. 2008;3(2):207-220.
39. Hoyt PR, Bartholomew C, Davis AJ, et al. The Evi1 proto-oncogene is required at midgestation for neural, heart, and paraxial mesenchyme development. *Mech Dev*. 1997;65(1-2):55-70.
40. Parkinson N, Hardisty-Hughes RE, Tateossian H, et al. Mutation at the Evi1 locus in Junbo mice causes susceptibility to otitis media. *PLoS Genet*. 2006;2(10):e149.
41. Zhang Y, Stehling-Sun S, Lezon-Geyda K, et al. PR-domain-containing Mds1-Evi1 is critical for long-term hematopoietic stem cell function. *Blood*. 2011;118(14):3853-3861.
42. Kataoka K, Sato T, Yoshimi A, et al. Evi1 is essential for hematopoietic stem cell self-renewal, and its expression marks hematopoietic cells with long-term multilineage repopulating activity. *J Exp Med*. 2011;208(12):2403-2416.
43. Saito Y, Kaneda K, Suekane A, et al. Maintenance of the hematopoietic stem cell pool in bone marrow niches by EVI1-regulated GPR56. *Leukemia*. 2013;27(8):1637-1649.
44. Yuasa H, Oike Y, Iwama A, et al. Oncogenic transcription factor Evi1 regulates hematopoietic stem cell proliferation through GATA-2 expression. *EMBO J*. 2005;24(11):1976-1987.
45. Yokomizo T, Ideue T, Morino-Koga S, et al. Independent origins of fetal liver haematopoietic stem and progenitor cells. *Nature*. 2022;609(7928):779-784.
46. Patel SH, Christodoulou C, Weinreb C, et al. Lifelong multilineage contribution by embryonic-born blood progenitors. *Nature*. 2022;606(7915):747-753.
47. Mazzi S, Lordier L, Debili N, Raslova H, Vainchenker W. Megakaryocyte and polyploidization. *Exp Hematol*. 2018;57:1-13.
48. Kuter DJ, Gminski DM, Rosenberg RD. Transforming growth factor beta inhibits megakaryocyte growth and endomitosis. *Blood*. 1992;79(3):619-626.
49. Bessman JD. The relation of megakaryocyte ploidy to platelet volume. *Am J Hematol*. 1984;16(2):161-170.
50. Levine RF, Hazzard KC, Lamberg JD. The significance of megakaryocyte size. *Blood*. 1982;60(5):1122-1131.
51. Thambyrajah R, Monteiro R. In the spotlight: the role of TGFβ signalling in haematopoietic stem and progenitor cell emergence. *Biochem Soc Trans*. 2022;50(2):703-712.
52. Brenet F, Kermani P, Spektor R, Rafii S, Scandura JM. TGFbeta restores hematopoietic homeostasis after myelosuppressive chemotherapy. *J Exp Med*. 2013;210(3):623-639.
53. Wu M, Chen G, Li YP. TGF-beta and BMP signaling in osteoblast, skeletal development, and bone formation, homeostasis and disease. *Bone Res*. 2016;4:16009.
54. Karsenty G, Wagner EF. Reaching a genetic and molecular understanding of skeletal development. *Dev Cell*. 2002;2(4):389-406.